

Back analysis and forecast of cave fragmentation at Cadia East mine

M. Fuenzalida^a, C. Orrego^b and E. Ghazvinian^a

^a*Itasca Consulting Group*

^b*Newmont Australia*

ABSTRACT

One of the key parameters impacting the performance and success of caving operations is rock fragmentation. Fragmentation directly affects productivity as it dictates hangup and secondary breakage events frequency and the likelihood of inrush events when percentage of fines is significant.

This paper outlines the methodology and results of a study aimed at forecasting fragmentation at Cadia East PC1-2/1-3 mine. The methodology employed in this study follows from previous methods (Pierce, 2010; Garza-Cruz et al., 2014; Fuenzalida et al., 2014; Pierce et al., 2022a) where a primary fragmentation nomogram is derived based on a series of numerical simulations conducted using the Synthetic Rock Mass (SRM) approach and estimates of secondary fragmentation are based on a shear-induced fragmentation logic included in the software *MassFlow* (Itasca, 2023).

A review of historical fragmentation data, including observations and measurements at drawpoints and beltcut, as well as hangup and secondary breakage frequency records is presented. The historical data is used as a metric to conduct a back-analysis of the predictive model. The results of this analysis suggest a strong correlation between historical data and model results. The model is then used to forecast fragmentation specifically, in terms of hang-up frequency and percentage of fines at PC1-2/PC1-3.

1 INTRODUCTION

One of the key parameters impacting the performance and success of a caving operation is rock fragmentation. Fragmentation dictates the diameter of draw zones and influences the mass flow behavior within the cave column, which in turn controls the rate of cave propagation, dilution entry, and resource recovery. Most importantly, fragmentation is directly related to productivity as it affects the frequency of hang-ups in the presence of large fragments and, it also affects the likelihood of mud rush events when the percentage of fines is considerable, and water is prevalent.

In general, two stages of fragmentation are considered: primary and secondary (see Figure 1). Primary fragmentation occurs in the cave back vicinity due to the effect of gravity or

induced stresses creating rock fragments through a combination of in-situ discontinuities, faults, veins and/or defects and growth of new fractures. Secondary fragmentation occurs within draw zones as rock fragments are subjected to high shear strains, causing further attrition (in the form of splitting and/or rounding) as they move down through the column. Impact onto muckpile when falling through air gap and compression in stagnant zones may be considered as other possible mechanisms during secondary fragmentation.

This paper outlines the results of a study aimed at forecasting the fragmentation at PC1-2 and PC1-3 at Cadia East mine. The methodology employed to derive fragmentation follows from previous methods based on numerical tools found in the literature (Pierce, 2010, Garza-Cruz et al., 2014, Fuenzalida et al., 2014, Pierce et al.,

2022a). A Synthetic Rock Mass (SRM)-based nomogram is used to provide estimates of primary fragmentation, and the software *MassFlow* (Itasca, 2023) is used to provide estimates of secondary fragmentation.

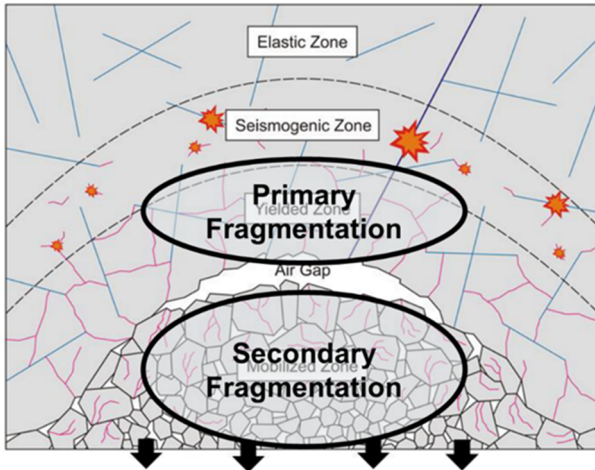


Figure 1 Primary and secondary fragmentation in a block cave mine (modified after Duplancic and Brady, 1999).

2 CADIA EAST MINE

Cadia East mine is one of Australia’s largest gold mining operations, located in New South Wales. The combination of a deep, high-stress environment, a competent rock mass and the ability to use very high lifts at depths between 1,200 and 1,400 m makes Cadia East unique compared to other operating cave mines. Establishment of Panel Cave 1 (PC1) at Cadia East commenced in early 2011 with its extraction level set at a depth of 1,200 m below the surface. Official production from PC1 began in 2013. Currently ore is extracted from PC1 and its neighboring panel (PC2) with an extraction level at 1,400 m depth. Plans to further develop panel caves for the Cadia East deposit are underway as extensions to the current PC1 and PC2 operations occur to the west (PC2-3) and East (PC1-2/PC1-3) caves, as shown in Figure 2.

3 NUMERICAL APPROACH TO CAVE FRAGMENTATION

The methodology applied to derive fragmentation outcomes for PC1-2 and PC1-3 follows from previous methods found in the literature (Pierce, 2010, Garza-Cruz et al., 2014,

Fuenzalida et al., 2014, Pierce et al., 2022a). As at many caving mines, a high degree of fragmentation variability and associated hangups and fines is observed at the drawpoints during life of mine (Moss et al, 2004; Pierce et al, 2022a). A unique characteristic of the methodology used for this study is that it captures the importance of strength and stress variability within the cave column, which in turn allows to provide estimates at more local scales across the footprint, i.e., at the panel, sector and drawpoint scales.

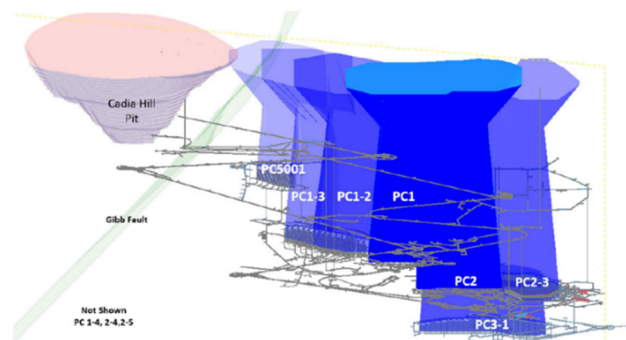


Figure 2 Location of PC1 and PC2 Caves. PC1-2/PC1-3 is located to the east of PC1.

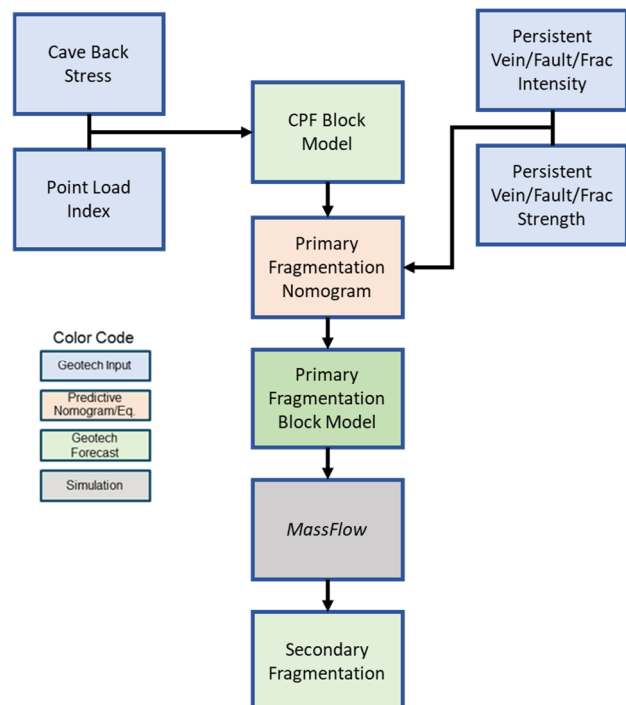


Figure 3 Main components of the cave fragmentation forecasting methodology modified after Pierce et al., 2022a.

The first step of the methodology is to obtain a primary fragmentation block model that will be used as input directly to *MassFlow*. As shown in Figure 3, the main inputs to derive a primary fragmentation block model are the cave back stress (CBS) and point load index (Is50) block models. In the case of a rock mass where persistent fractures (e.g., open joints, weak veins, hydrofractures etc.) are present, the effective persistent fracture intensity (P32eff) block model should be considered given its importance in the creation of fragments, especially when these persistent features are weaker than the host strength. Once a primary fragmentation model has been created, this is used as input in *MassFlow* and secondary fragmentation curves are estimated using the Bridgwater shear-induced attrition model (Bridgwater et al., 2003, Pierce, 2010) that is embedded in *MassFlow*.

3.1 Primary Fragmentation

The SRM-based primary fragmentation nomogram (Figure 3) is used to estimate the primary fragmentation in each block from the local estimates of CBS, Is50h (Is50 host strength) and the intensity of the persistent discontinuities, P32eff. As described in Pierce et al. (2022a), the nomogram (Figure 3) was derived from a series of SRM testing of large-scale [20 m (span) x 10 m (height) x 12 m (width)] rock mass samples built in *3DEC* (Itasca, 2023) containing persistent weak veins, open joints, small-scale faults, and hydraulic fractures represented via Discrete Fracture Networks (DFNs). The SRM sample that hosts the DFN is comprised of an assembly of tetrahedral-shaped blocks with contact strengths defined by Is50h. Fragmentation potential is estimated by subjecting SRM samples to a range of CBS and deconfining from the bottom to mimic the advance of the cave back. The ratio of CBS to Is50h*11.5, forming the x-axis of the nomogram, is also termed the Cave Propagation Factor (CPF) and is a metric for fragmentation potential in the absence of weak, persistent structures. The empirical factor of 11.5 in the

denominator sets the onset of fragmentation at CPF=1 when P32eff=0. As indicated by the nomogram, fragmentation is directly related to CPFs; in the case of low CPFs fragmentation is expected to be coarser, and in the case of high CPFs, fragmentation is expected to be finer. The Weibull distribution is used to describe fragment volume distributions within the methodology because of its versatility to fit different levels of skewness. The output from the nomogram is the Weibull scale parameter of the primary fragmentation distribution, η , which can be input with the Weibull shape parameter, β , (estimated at 2.5¹) to the cumulative density function. This defines the percentage of fragments (by volume) passing a given volume, V , as:

$$F(V[m^3])=1-\exp[-((V[m^3]/\eta)^\beta)] \quad (1)$$

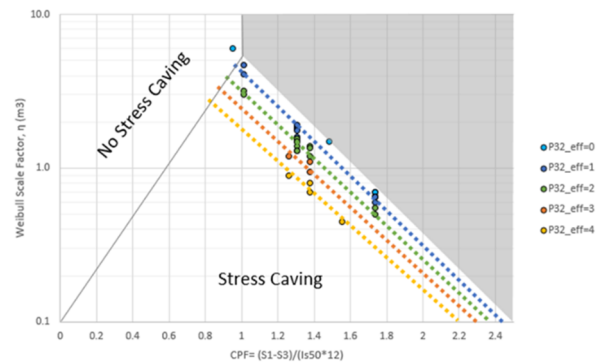


Figure 4 SRM-based primary fragmentation nomogram (Pierce et al., 2022a).

3.2 Secondary Fragmentation

MassFlow, as its predecessor *REBOP*, models flow by tracking the growth of the isolated movement zones (IMZ) and the internal material movement associated with draw.

Secondary fragmentation in *MassFlow* is processed by systematically reducing the fragment size² associated with markers based on their tensile strength, stress and shear strain experienced as they transit through the IMZ toward the drawpoint (Figure 5).

The core scale tensile strength associated with a given marker is selected randomly from the Weibull distribution derived from point load

¹ A Weibull distribution with a shape parameter of 2.5 behaves closely to a normal distribution.

² Fragment size is defined as the largest dimension of a rock fragment.

block model. As indicated in the previous section, this random assignment relies on the block model of point load index that quantifies distribution of point load index in each block, not just the mean value.

There is strong empirical evidence that rock strength will decrease as the scale increases following a power-law decay (e.g., see Fuenzalida et al, 2022). The core scale tensile strength is scaled as a function of rock block size assuming a power-law decay towards the rock mass scale (Figure 6). Equations 2-5 show the power-law decay functions employed to assess scale effects during tensile strength assignment as a function of fragment size. The scale at core and rock mass scales are assumed as 50mm and 10m respectively. The tensile strength at core scale (T_{core}) is assigned using the Weibull distribution in the point load index block model. The tensile strength at rock mass scale (T_{rm}) is determined based on Equation 3.

$$T = n \text{ scale}^{-k} \quad (2)$$

$$T_{rm} = 0.2 * \eta * (1 + \ln(\beta)) \quad (3)^3$$

$$k' = - \frac{\log T_{core} - \log T_{rm}}{\log \text{scale}_{core} - \log \text{scale}_{rm}} \quad (4)$$

$$n' = 10^{(\log T_{core} - k' * \log \text{scale}_{core})} \quad (5)$$

where:

T_{core} = tensile strength at core scale.

T_{rm} = tensile strength at rock mass scale.

scale_{core} = core scale assumed as 50mm.

scale_{rm} = rock mass scale assumed as 10m.

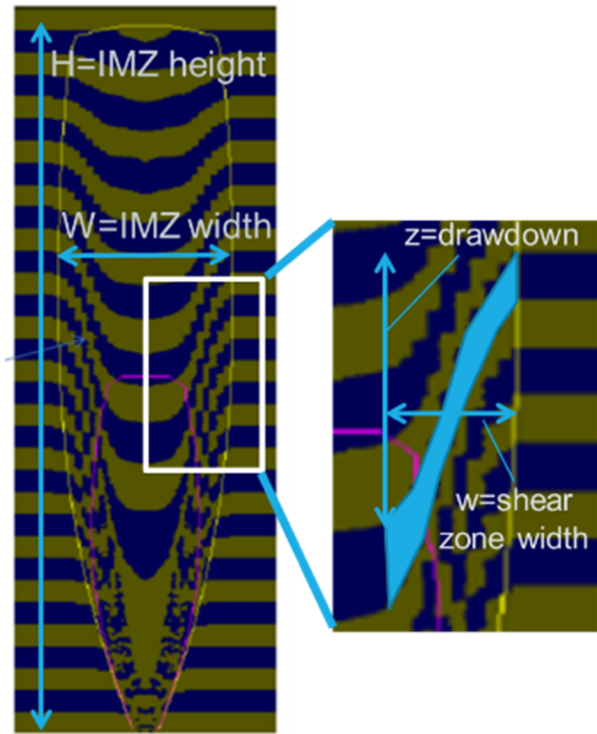


Figure 5 Shear strain as fragments transit through the IMZ towards drawpoints (modified from Pierce, 2010).

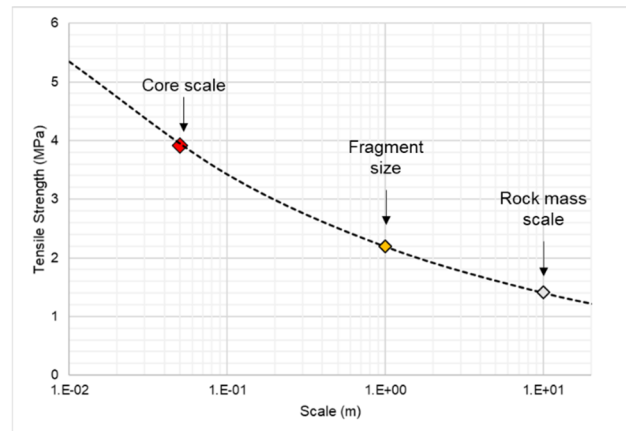


Figure 6 Power law relationship of scale effect implemented in MassFlow.

The degree of breakage experienced by a rock fragment moving inside of the draw zone is a function of the average normal stress inside the IMZ relative to the strength of the fragments and the incremental shear strain. *MassFlow* has embedded the shearing attrition model developed by Bridgwater et al. (2003):

³ Scale η and shape β parameters are determined from Weibull distribution representing point load index at the

core scale. Scale parameter has units of MPa. Equation based on the work from Pierce et al. (2022b)

$$W = K \left(\frac{\sigma_n \cdot \Gamma^\phi}{\sigma_t} \right)^\beta \quad (6)$$

Where:

W = mass fraction attrited from a mono-sized initial assembly (%);

σ_n = normal stress applied to the assembly (MPa);

Γ = accumulated shear strain applied to the assembly (dimensionless);

σ_t = tensile strength of the constituent particles in the assembly (MPa); and

K, ϕ, β = empirical constants (dimensionless).

4 MODEL INPUTS

As described in Section 2, to use the primary fragmentation nomogram three main inputs are necessary: 1) Is50 block model, 2) cave back stress (CBS)⁴ block model, and 3) a P32 of persistent features block model. The following section describes the point load index and cave back stress block models.

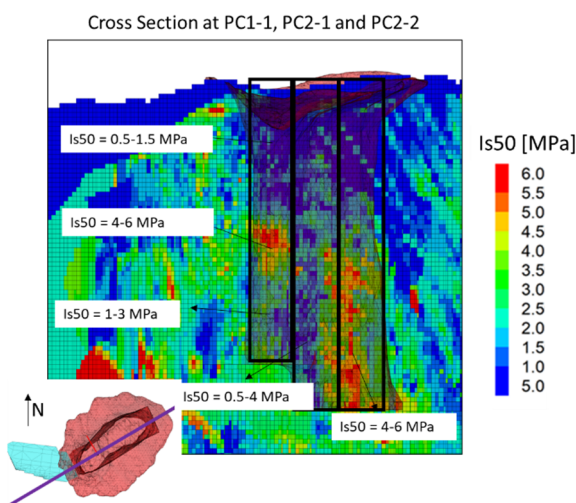


Figure 7 Section of point load index (MPa) – Scale parameter – 63rd percentile at PC1 and PC2.

4.1 Point Load Index Block Model

A systematic point load test (PLT) campaign was carried out by Cadia East in PC1-2 footprint and ore column during 2020. Using machine learning, Cadia East was able to populate the entire drillhole database and create an Is50 block model (Pierce et al., 2022b). The Is50 block model provides evidence of the strength heterogeneity within the cave footprint and column at Cadia. Overall, the rock mass shows a wide range of point load strengths varying between 0.5-6 MPa. In general, the top part of the cave column is characterized with lower strengths with Is50 between 0.5-1.5 MPa. The lower half of the column of PC1-1, PC2-1 and PC2-2 shows very different strength characteristics with PC2-2 having a more competent stronger rock mass (Is50 between 4-6 MPa) than PC2-1 (Is50 between 0.5-4 MPa) and PC1-1 (Is50 between 1-3 MPa) (see Figure 7). PC1-2 and PC1-3 cave columns are less variable. PC1 and PC2, although, sectors of weak (less than 2 MPa) and strong (greater than 5 MPa) can be observed spatially distributed in both cave columns as shown in Figure 8. The Is50 block model is also a key input for the secondary fragmentation stage in the methodology as it is used to assign tensile strength in the attrition model implemented in *MassFlow*.

4.2 Cave Back Stress Block Model

As the cave propagates and breaks through the surface, the magnitude and orientation of the principal stresses at onset of rock mass yield is recorded. Cave back stress (CBS) is defined as the magnitude of the deviatoric stress, difference between the major and minor principal stress at onset of yield. Overall, cave back stresses can be quite heterogeneous as the cave propagates through the column (Figure 9). The cross-section along PC1 and PC2 shows elevated stresses (~50-70 MPa) at the intersection between PC1 and PC2 as well as in the initiation point for each cave in the lower part of the column. As expected, stresses are in the lower range (5-30

⁴ In this study, an elasto-plastic numerical model was used to determine the CBS block model.

MPa) near the surface. A section crossing at PC1-2 and PC1-3 (Figure 10) shows a similar pattern to the existing caves. Elevated stresses (50-70 MPa) are concentrated around cave boundaries at the base of the column where the local influence of the preexisting PC1-1 prior to the start of PC1-2 is observed, and lower stresses (5-30 MPa) are observed in the upper part of the column.

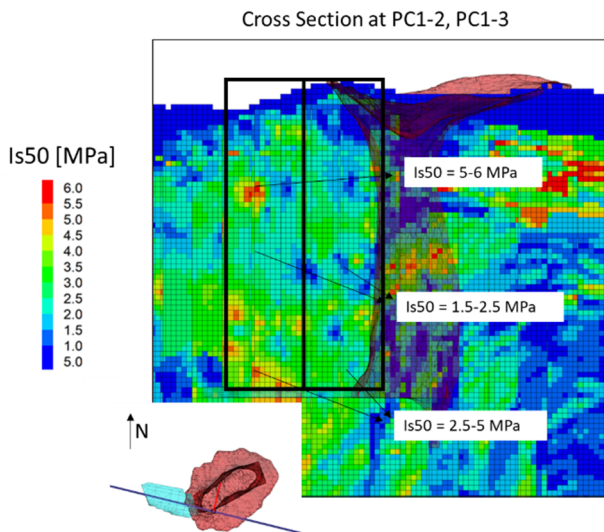


Figure 8 Section of point load index (MPa) at PC1-2/PC1-3.

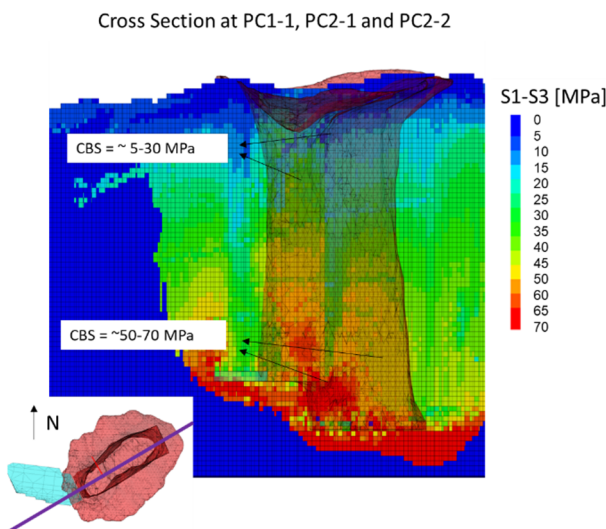


Figure 9 Section of cave back stress block model at PC1 and PC2.

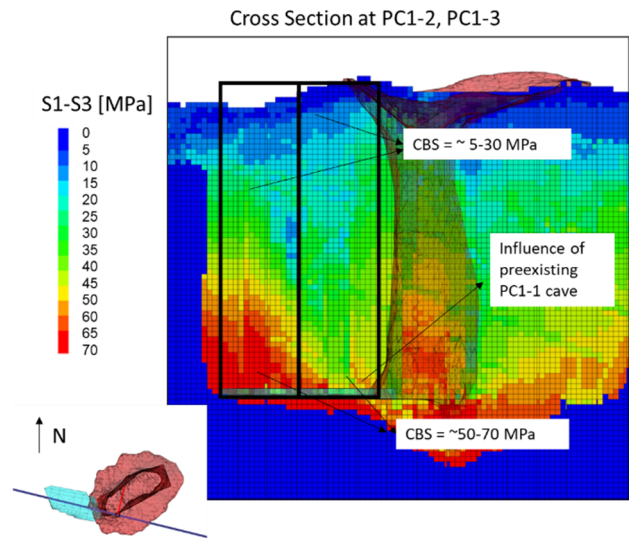


Figure 10 Section of cave back stress block model at PC1-2 and PC1-3.

4.3 Intensity of Persistent Features - P32eff

The impact of the intensity of persistent features (P32eff), which includes weak veins, open features, and hydraulic fractures on oversize (%) is variable and relies on local CPF estimates within each block. Figure 11 illustrates this relationship, showing a graph that quantifies the effect of P32eff in the x-axis and the resulting oversize (%) for a given CPF value.

Given the high degree uncertainty within the Cadia East P32eff block model, a sensitivity analysis was conducted. This analysis presumed uniform spatial distribution of P32eff values throughout the entire rock mass at Cadia East. The results discussed in Section 6.0 used a P32eff constant of 3 (1/m).

5 CADIA EAST HISTORICAL FRAGMENTATION DATA

A review of Cadia East historical fragmentation data was conducted that looked at observations and actual measurements of 1) drawpoint fragmentation, 2) beltcut fines measurements, 3) hangup and secondary breakage frequency counts.

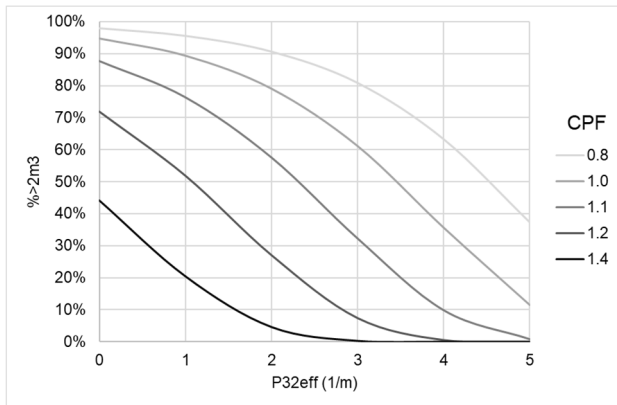


Figure 11 Effect of P32eff on oversize (%) for varying CPF values.



Figure 12 Extracted fragments from drawpoint 118W05 (PC1-1) at HoD~265m (Newcrest, 2019).

5.1 Drawpoint Fragmentation Curve Measurements

In the past, Cadia East has employed optical photogrammetry for assessing drawpoint fragmentation. However, like all photogrammetry techniques, this method is prone to errors, often resulting in underestimation of fines percentage. To address this limitation, a comprehensive test work program was conducted in 2019 to enhance the accuracy of fragmentation measurement at various stages of drawpoint maturity. The test work involved trucking 50T of material samples to surface from three different drawpoints, each at different heights of draw (HoD). Photographs and scans were collected of the full piles and from within loader buckets. Samples were restacked and the process repeated. The material was then trucked offsite for physical sieving of the three samples (Newcrest, 2019). Figure 11 shows an example of the extracted fragments from drawpoint 118W05 (PC1-1) at HoD ~265m. The resulting fragmentation curves of

the three samples are shown in Figure 12. Despite originating from different Panels (PC1-1, PC2-1, and PC2-2), the impact of HoD is evident in the evolving fragmentation curves, transitioning from coarse to fine as HoD increases.

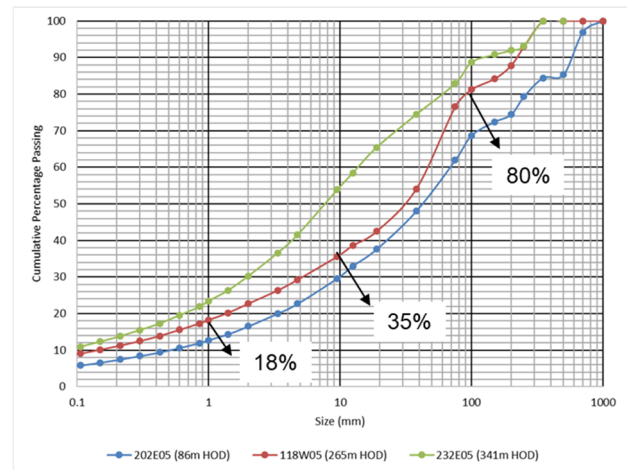


Figure 13 Fragmentation curves from physical sizing on drawpoints 202E05(PC2-2), 118W05 (PC1-1), and 232E05(PC2-1) at different HoD.

5.2 Beltcut measurements

The crusher output, beltcut, is sampled and sieve analysis is performed approximately every three months to derive a particle size distribution. The most recent dataset considered for validating the model results is from December 2021. Given that each Panel (PC) has a unique crusher, this data presents an excellent opportunity to discern differences in fragmentation fines between panels. Beltcut data offer a more dependable measure of fine material arriving at the drawpoints. For comparative analysis, a fragment diameter of 9.5mm was selected, as fragments of this size remain unaffected by the crusher's opening (Bear Rock Solutions, 2022).

Figure 13 shows the percentage passing (%<) 9.5mm evolution (actuals) with increasing HoD for PC1-1, PC2-1, and PC2-2. The percentage less than 9.5 mm shows that PC1-1 tends to be finer than PC2-1 and PC2-2.

5.3 Hangup and secondary breakage frequency

Hangup and secondary breakage frequency is defined as the number of hangups, or secondary

breakage events every 1000 tonnes extracted. The hangup and secondary breakage events, i.e., an event is defined as the successful removal of a hangup, are summed and classified based on HoD. Figure 14 shows the actual frequency of PC1-1, PC2-1, and PC2-2. The plot shows that PC1-1 and PC2-1 behaved similarly with a low event frequency (0.2-0.5 events/1000t) while PC2-2 shows a higher event frequency (1-1.3 events/1000t) for HoD less than 200m. Differences between PC2-2 and PC2-1/PC1-1 hangup and secondary breakage frequency provide evidence of the importance in capturing the strength and stress variability across the cave column.

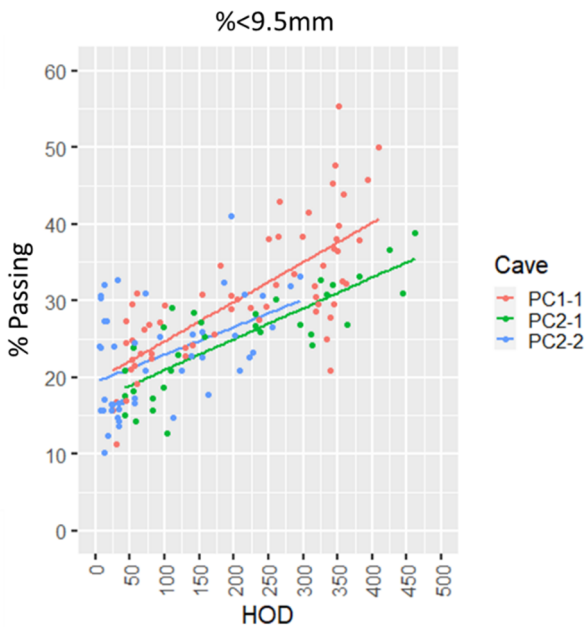


Figure 14 Belt cut measurements of %<9.5mm versus HoD(m).

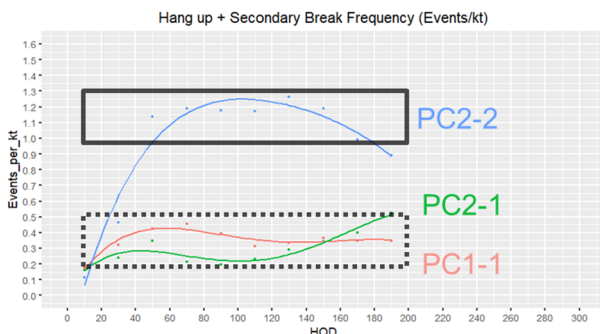


Figure 15 Actual hangup and secondary breakage events as function of HoD for PC1-1, PC2-1, and PC2-2.

6 MODEL RESULTS COMPARISON AGAINST ACTUAL DATA

MassFlow reports results of fragmentation as particle size distributions per drawpoint over the life of mine. The model was run using the future draw schedule for PC1-2/PC1-3 as well as for current active Panels PC1-1, PC2-1, and PC2-2.

6.1 Drawpoint Fragmentation Curve Measurements

A comparison of the fragmentation curves of the sampled drawpoints from PC1-1, PC2-1 and PC2-2 was done against the model by considering the results of each individual panel at the specific height of draw when these drawpoints were sampled. Figure 15 shows the comparison of fragmentation curves between physical sizing (continuous lines) and model (dashed lines) for the three sampled drawpoints of PC1-1, PC2-1, and PC2-2 at corresponding HoD. Overall, the match between model and measurements is reasonable, where the difference between each curve is within ~10% of error. The major difference is observed in PC2-2 where the emergent fragmentation curve shows a coarser fragmentation for the upper sizes than the actual observations. This might be attributed to that the loader bucket is restricted to carry a certain material upper size based on its volume (~10m³) impeding hauling larger sizes to surface.

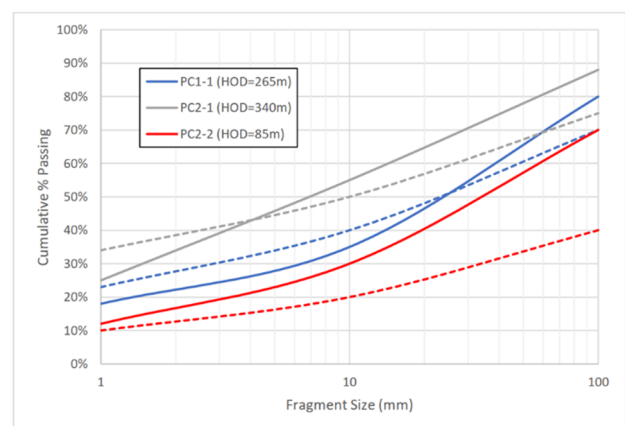


Figure 16 Comparison of fragmentation curves between physical sizing (continuous lines) and model (dashed lines) for selected drawpoints of PC1-1, PC2-1, and PC2-2 at different HoD.

6.2 Hangup and secondary breakage frequency

In the model, the hangup and secondary breakage frequency are calculated based on the number of fragments arriving at the drawpoints that have a diameter greater than 2m. This size was selected based on bucket capacity and operational standards to avoid ROM bin blockages. Figure 17 shows the model results plotted using the same window of observation as the historical event frequency. Overall, the model shows that PC2-2 matches well with actuals, while for PC2-1 and PC1-1, the model tends to slightly overestimate the event frequency although both curves are within the range of observations. The distinct behavior of PC2-2 is well captured by the model, which demonstrate the importance of properly representing the strength and stress heterogeneity at Cadia East.

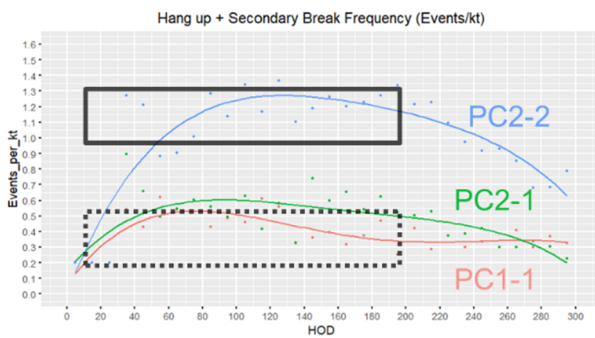


Figure 17 Model hangup and secondary breakage events as a function of HoD for PC1-1, PC2-1, and PC2-2.

6.3 Beltcut measurements

Model fragmentation results are presented as whisker plots of percentage less than 9.5mm to understand drawpoint variability with increasing HoD. The box and whisker represent the variability associated with all drawpoints corresponding to each Panel. Figure 17, Figure 18, and Figure 19 show whisker plots for PC1-1, PC2-1 and PC2-2 respectively where black dots are the actual measurements. Overall, the results indicate that the model provides a good match for PC1-1, although it tends to overestimate PC2-1 and slightly underestimate PC2-2 in the first 100m of HOD. Given that beltcut

measurements are taken with a periodicity of approximately every 3 months, there is an intrinsic variability associated with this data, the model results are considered to be in line with observed fines at Cadia East.

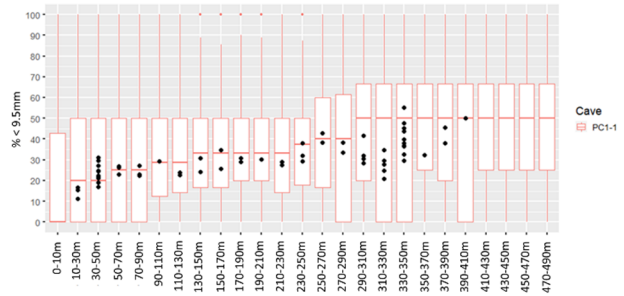


Figure 18 PC1-1 whisker plot showing drawpoint variability of % < 9.5mm versus HOD. Actual values in black dots.

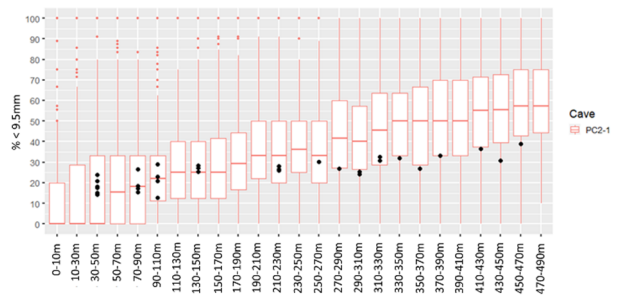


Figure 19 PC2-1 whisker plot showing drawpoint variability of % < 9.5mm versus HOD. Actual values in black dots.

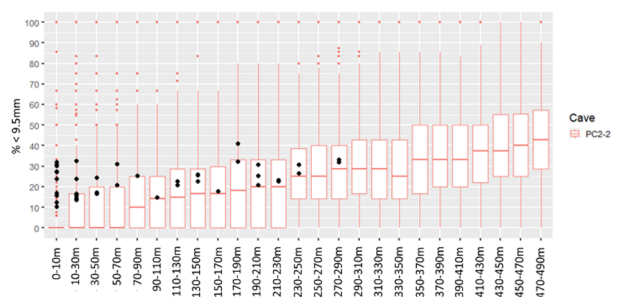


Figure 20 PC2-2 whisker plot showing drawpoint variability of % < 9.5mm versus HOD. Actual values in black dots.

7 FORECAST OF CAVE FRAGMENTATION AT PC1-2/PC1-3

Drawpoints corresponding to each Panel are classified based on their HoD so that side-by-

side comparisons between different Panels can be done (Figure 10). All Panels show the expected behavior of a decrease in frequency of events as HoD increases with PC2-2 showing the highest with a peak of 1-1.3 events/1000T at 150m of HoD while PC1-1 shows the lowest with a peak of 0.4-0.5 events/1000T at ~100m HoD. The forecast suggest to PC1-2 would behave like PC2-1 while PC1-3 shows more variability with increasing HoD, but still it is expected to experience less hangups and secondary breakage than PC2-2.

In terms of fines forecasting, the 9.5mm was the fragment size chosen to quantify the fines portion at Cadia East. Whisker plots of percentage less than 9.5mm are created considering all active PC1-2/PC1-3 drawpoints classified based on their HoD. As expected, both PC1-2 and PC1-3 show that fines increase with HoD (Figure 22 and Figure 23). When compared to PC1-1 actuals (black dots), both Panels are expected to behave similarly to PC1-1 fines with increasing HoD.

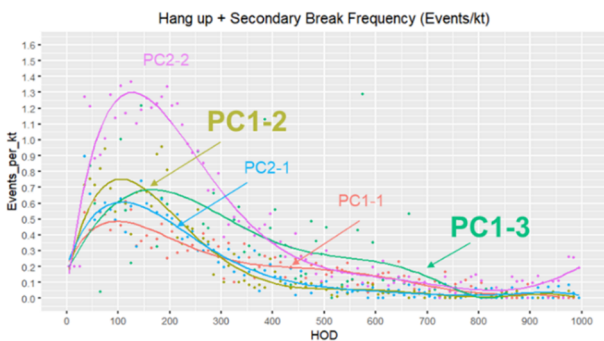


Figure 21 Forecast of hangup and secondary breakage frequency.

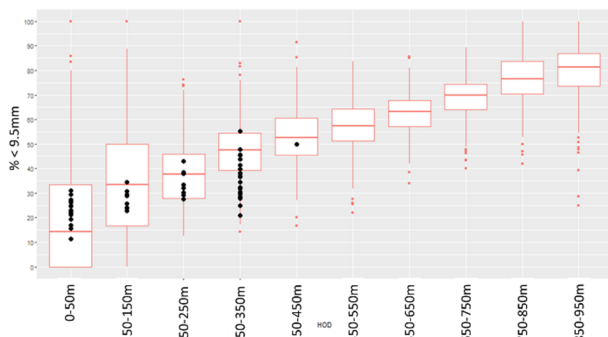


Figure 22 Whisker plot showing % < 9.5mm for PC1-2 with increasing HoD (m). PC1-1 actual values shown in black dots.

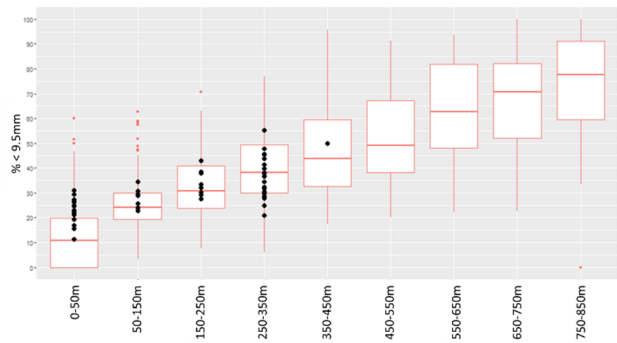


Figure 23 Whisker plot showing % < 9.5mm for PC1-3 with increasing HoD (m). PC1-1 actual values shown in black dots.

8 CONCLUSIONS

A fragmentation assessment has been conducted making use of the latest information available of the Cadia East orebody. The point load index block model is a key input to the fragmentation methodology implemented in this study as it allows the capture of the strength heterogeneity present at the Cadia East orebody. This methodology also uses as input the cave back stress block model from the numerical model which provides another source of heterogeneity during cave propagation and interaction with previous caves. Both sources of heterogeneity are key inputs of this methodology providing an opportunity to conduct a panel-based assessment of fragmentation.

A comparison to site observations has been made including drawpoint and beltcut observations, hangup, and secondary breakage frequency, and drawpoint fragmentation measurements. Overall, the model agrees well with actual measurements and observations providing enough confidence for it to be used as a forecasting tool for PC1-2 and PC1-3.

The forecast shows that PC1-2 and PC1-3, in terms of hangup and secondary breakage frequency, would behave similarly to PC2-1, which in relative terms, is finer than PC2-2 and a bit coarser than PC1-1. In terms of fines (% < 9.5mm), both Panels would behave similarly to PC1-1.

Although, the role of HF was not explicitly included in the model, the intensity of hydraulic fractures may be accounted as part of the P32eff

assumptions used in the primary fragmentation block model. Future work should include running SRM models to include explicitly the effects of hydraulic fractures in the primary fragmentation estimates.

Hangup frequency and secondary breakage events do not solely depend on oversize material but are also dependent on operational constraints such as drawbell geometry, draw rates, type of equipment, etc. Selection of 2m fragment diameter threshold to relate hangup and secondary breakage frequency showed a good correlation to site experience. This threshold should be carefully revisited when using a similar methodology at other sites.

Point load index and cave back stress block models used as inputs to the methodology described in this paper inherently carry assumptions and errors. Uncertainty associated with each step in the process of development of the point load index block model should be considered when applying these types of models to rock strength and fragmentation predictions to mine design studies. In addition, uncertainty associated with the CBS block model should also be considered as stresses obtained to create such a model come from a continuum numerical model that does not include local changes to modulus nor explicit representation of small-scale discontinuities and/or defects present in the rock mass that could affect stress redistribution around the cave.

ACKNOWLEDGEMENTS

The authors thank Newmont for allowing the publication of this paper.

REFERENCES

- Bridgwater, J., Utsumi, R., Zhang, Z. & Tuladhar, T. (2003). Particle Attrition Due to Shearing—the Effects of Stress, Strain and Particle Shape. *Chem. Eng. Sci.*, 58, 4649–4665.
- Bear Rock Solutions, (2022). Addition of Primary Crusher Model to REBOP Drawpoint Fragmentation. Comments Following PoC Implementation'. PowerPoint Presentation.
- Duplancic, P. & Brady B. H. (1999) Characterization of caving mechanisms by analysis of seismicity and rock stress. Paper presented at the 9th ISRM Congress, Paris, France, August 1999.
- Fuenzalida, M. A., Orrego, C., Ghazvinian, E. & Pierce, M. E. (2022). Application of rock mass strength scale effect at Cadia East mine. in Y Potvin (ed.), *Caving 2022: Proceedings of the Fifth International Conference on Block and Sublevel Caving*, Australian Centre for Geomechanics, Perth, pp. 951-962, https://doi.org/10.36487/ACG_repo/2205_65.
- Fuenzalida, M., Garza-Cruz, T., Pierce, M. & Andrieux, P. (2014) Application of a methodology for secondary fragmentation prediction in cave mines. in *Proceedings, 3rd International Symposium of Block and Sublevel Caving* (Santiago, Chile, June 2014).
- Garza-Cruz, T., Fuenzalida, M., Pierce, M. & Andrieux, P. (2014). A 3DEC-FALC3D Model to predict primary fragmentation distribution in Cave Mines. in *Proceedings, 3rd International Symposium of Block and Sublevel Caving* (Santiago, Chile, June 2014).
- Itasca Consulting Group, Inc. (2023). 3DEC — Three-Dimensional Distinct Element Code (Version 9.0). Minneapolis: Itasca.
- Itasca Consulting Group Inc. (2023). MassFlow (Version 9.0). Minneapolis: Itasca.
- Pierce, M. (2010). A Model for Gravity Flow of Fragmentated Rock in Block Caving Mines. Ph.D. Thesis, University of Queensland.
- Pierce, M. E., Llewelyn, K., Campbell, R., Taylor, K., Fuenzalida, M. A. & Diering, M. (2022a). Development, reconciliation and visualisation of hang-up frequency and fines entry forecasts at PT Freeport Indonesia. in Y Potvin (ed.), *Caving 2022: Proceedings of the Fifth International Conference on Block and Sublevel Caving*, Australian Centre for Geomechanics, Perth, pp. 531-544, https://doi.org/10.36487/ACG_repo/2205_36.
- Pierce, M. E., Stonestreet, P., Orrego, C., Tennant, D., Garza-Cruz, T. V., Furtney, J. & Thielsen, C. (2022b). Development of rock mass strength block models at Cadia East mine. in Y Potvin (ed.), *Caving 2022: Proceedings of the Fifth International Conference on Block and Sublevel Caving*, Australian Centre for Geomechanics, Perth, pp. 1033-1046, https://doi.org/10.36487/ACG_repo/2205_71.